

BRIGHT: A globally distributed multimodal building damage assessment dataset with very-high-resolution for all-weather disaster response

Hongruixuan Chen^{1,2}, Jian Song^{1,2}, Olivier Dietrich³, Clifford Broni-Bediako², Weihao Xuan^{1,2}, Junjue Wang¹, Xinlei Shao¹, Yimin Wei¹, Junshi Xia², Cuiling Lan⁴, Konrad Schindler³, and Naoto Yokoya^{1,2}

¹Graduate School of Frontier Sciences, The University of Tokyo, Chiba, Japan

²RIKEN Center for Advanced Intelligence Project (AIP), RIKEN, Tokyo, Japan

³Department of Photogrammetry and Remote Sensing, ETH Zürich, Zürich, Switzerland

⁴Microsoft Research Asia, Beijing, China

Correspondence: Naoto Yokoya (yokoya@k.u-tokyo.ac.jp)

Abstract. Disaster events occur around the world and cause significant damage to human life and property. Earth observation (EO) data enables rapid and comprehensive building damage assessment, an essential capability in the aftermath of a disaster to reduce human casualties and to inform disaster relief efforts. Recent research focuses on the development of artificial intelligence (AI) models to achieve accurate mapping of unseen disaster events, mostly using optical EO data. However, solutions based on optical data are limited to clear skies and daylight hours, preventing a prompt response to disasters. Integrating multimodal EO data, particularly the combination of optical and synthetic aperture radar (SAR) imagery, makes it possible to provide all-weather, day-and-night disaster responses. Despite this potential, the development of robust multimodal AI models has been constrained by the lack of suitable benchmark datasets. In this paper, we present a Building damage assessment dataset using very-high-resolution optical and SAR imagery (BRIGHT) to support AI-based all-weather disaster response. To the best of our knowledge, BRIGHT is the first open-access, globally distributed, event-diverse multimodal dataset specifically curated to support AI-based disaster response. It covers five types of natural disasters and two types of man-made disasters across 12 regions worldwide, with a particular focus on developing countries where external assistance is most needed. The optical and SAR imagery in BRIGHT, with a spatial resolution between 0.3 and 1 meters, provides detailed representations of individual buildings, making it ideal for precise damage assessment. In our experiments, we have tested seven advanced AI models trained with our BRIGHT to validate the transferability and robustness. The corresponding experimental results can also serve as a baseline for future research, providing perspectives and inspiration for the design of custom models. The dataset, along with code and trained models, is available at <https://github.com/ChenHongruixuan/BRIGHT>, and will be updated as new disaster data become available. BRIGHT also serves as the official dataset for the 2025 IEEE GRSS Data Fusion Contest Track II. We hope that the new dataset will further the use of AI-driven EO methods in support of people in disaster-affected areas.

1 Introduction

A disaster is defined as a serious disruption in the functioning of a community or society due to the interaction between a hazard event and the conditions of exposure, vulnerability, and capacity; resulting in human, material, economic, or environmental losses and impacts (Ge et al., 2020). According to (UNDRR, 2018a), three types of natural disasters – earthquakes, storms, and floods – have caused ≈ 1.12 million deaths, affected 2.85 billion people, and resulted in more than 2,647 billion US dollars in economic losses between 1998 and 2017. The threat of disasters is likely to increase as a result of global urbanization. Rapid and comprehensive damage assessment is crucial in the aftermath of a disaster to make informed and effective rescue decisions and minimize losses and impacts. Among these assessments, building damage assessment, aiming at providing information including the area and amount of damage, the rate of collapsed buildings, and the type of damage incurred by each building, is particularly critical in the early stages. This is because the distribution of damaged buildings is closely related to life-saving efforts in emergency response (Xie et al., 2016; Adriano et al., 2021). However, conducting field surveys after a disaster is difficult and dangerous, especially when transportation and communication systems are disrupted, impeding efficient on-site assessments. Earth observation (EO) technology, also known as remote sensing, provides a safe and efficient way to obtain building damage information over disaster areas due to its wide field-of-view, low cost, and contactless operation.

Two primary types of EO technology, optical and synthetic aperture radar (SAR), are commonly used for assessing building damage after disasters. Optical EO imagery has been the primary source and has been extensively studied for building damage assessment, because of its intuitive and easy-to-interpret nature. Initially, moderate-resolution optical EO data, exemplified by the Landsat series and Sentinel-2, was used for assessing building damage (Yusuf et al., 2001; Fan et al., 2019; Sandhini Putri et al., 2022). However, these were limited by spatial resolution and only provided broad approximations of affected areas, lacking accuracy for specific buildings, which is crucial for timely rescue. The new generation of very-high-resolution (VHR) optical sensors, such as IKONOS and WorldView, provide EO data with spatial resolutions at the meter and even sub-meter level, enabling finer assessments at the level of individual buildings (Freire et al., 2014). These data have been successfully used for building damage assessment after multiple natural disasters (Yamazaki and Matsuoka, 2007; Tong et al., 2012; Freire et al., 2014). While accurate building damage proxy maps can be obtained through visual interpretation by experts, this process is time-consuming, requires trained professionals, and is in practice too labor-intensive for rapid, large-scale assessments. Therefore, much of the recent literature has focused on developing automated methods for rapid building

damage proxy mapping (Tong et al., 2012; Xie et al., 2016; Gupta et al., 2019; Zheng et al., 2021). Among these, artificial intelligence (AI), especially deep learning (DL) techniques, have proved particularly effective, significantly improving the efficiency and accuracy of building damage assessments. Early works were often specific to a single disaster event, with labels annotated for a particular disaster area to train the model, which was then used to generate building damage proxy maps for the same event (Xie et al., 2016; Xia et al., 2023). Since the associated training sets are limited to a narrow range of building types, damage patterns, and background land-cover distributions, the resulting models lack generalizability and struggle to produce accurate building damage proxy maps for new disaster events, which limits their practical use. The release of large-scale benchmark datasets including a variety of disaster scenarios and damage types, such as the xBD dataset (Gupta et al., 2019), opens up the possibility of using DL models to quickly and accurately map building damages after a newly occurred, previously unseen disaster. A number of state-of-the-art methods based on various DL models have been designed (Zheng et al., 2021; Shen et al., 2022; Guo et al., 2024; Wang et al., 2024; Chen et al., 2022; Kaur et al., 2023; Chen et al., 2024). For example, Zheng et al. (2021) trained DL models on the xBD dataset and applied them to mapping building damages on two unseen man-made disaster events. These studies showcase the power of employing DL models for building damage mapping. However, optical EO, being a passive sensing technique, needs suitable solar illumination and cloud-free weather conditions, which severely limits its application as an emergency tool for all-weather disaster response (Adriano et al., 2021). Actual disaster events, especially wildfires, floods, and storms, are often accompanied by less-than-ideal imaging conditions. For instance, Figure 1 shows EO data captured for a wildfire event that occurred in August 2023 in Hawaii, USA. The post-event optical image shown in Figure 1b does not provide clear surface information due to the effects of smoke from the wildfire. In contrast, SAR sensors employ active illumination with longer microwaves and can acquire images in adverse weather conditions, offering great potential for all-weather disaster response. As illustrated in Figure 1c, SAR imagery is unaffected by smoke and clearly shows buildings damaged by the wildfire.

Due to the above advantages of SAR data and the development of associated processing technology, various SAR-based methods have been proposed for assessing building damage. These methods utilize intensity (Matsuoka and Yamazaki, 2005, 2010; Matsuoka et al., 2010), coherence (Yonezawa and Takeuchi, 2001; Arciniegas et al., 2007; Watanabe et al., 2016; Liu and Yamazaki, 2017), or polarization features (Yamaguchi, 2012; Chen and Sato, 2013; Watanabe et al., 2016; Karimzadeh and Matsuoka, 2017) for the building damage assessment at the block unit level, depending on the acquisition mode. Several studies have attempted to extend the block-level approach or have explored

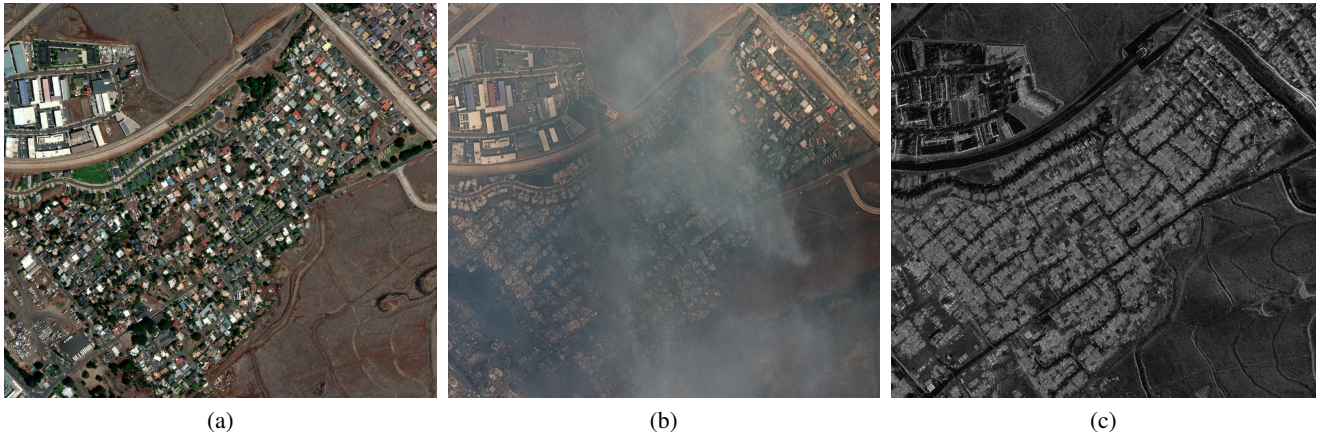


Figure 1. An example of the wildfire occurring in Maui, Hawaii, USA, August 2023. (a) Pre-event optical imagery (© Maxar). (b) Post-event optical image (© Maxar) with land-cover features obscured by smoke from wildfires. (c) Post-event SAR imagery (© Capella Space) unaffected by smoke, clearly showing disaster area.

new approaches to move towards building instance level, using higher spatial resolution sensors like COSMO-SkyMed and TerraSAR-X (Liu et al., 2013; Brett and Guida, 2013; Chini et al., 2015; Ge et al., 2019). Some studies have also explored AI-based approaches for building damage assessment based on SAR data (Bai et al., 2018; Adriano et al., 2019; Bai et al., 2017; Li et al., 2023b). However, due to the lack of large-scale benchmark datasets (like xBD in the optical domain), these methods have focused on local regions and single disaster events, and their ability to generalize to other disaster events remains largely unknown. Challenges inherent to SAR data, such as oblique viewing angles, speckle noise, object occlusion, and geometric distortions, complicate the accurate mapping of buildings compared to optical imagery (Brunner et al., 2010; Adriano et al., 2021). Additionally, the limited availability of VHR SAR data also reduces its reliability as a source of pre-event data (Brunner et al., 2010). Considering these practical limitations, the most effective strategy for rapid, all-weather building damage assessment might arguably be to combine pre-event optical imagery, which provides accurate localization and detailed building information in the visible spectrum, with post-event SAR imagery, which captures structural information as a cue for building damages (Adriano et al., 2019). However, the image formation of SAR differs from that of an optical camera, both in terms of the physical properties of the imaged targets and in terms of the signal processing steps to create the image. Previous methods have attempted to align the two modalities with manually constructed statistical models (Stramondo et al., 2006; Chini et al., 2009; Brunner et al., 2010; Wang and Jin, 2012). However, these models are sensor-specific, requiring dedicated modeling for each sensor. DL offers a promising solution by automatically learning a high-dimensional feature space that aligns the two modalities. Still, a significant challenge remains: to train and eval-

uate a DL model, one must have access to a high-quality, large-scale dataset with comprehensive coverage of various disaster events and sufficient geographic diversity.

To support AI research aimed at all-weather building damage mapping, we present BRIGHT, the first open, globally distributed, multimodal VHR dataset for building damage assessment. Advances in EO technology have enabled data providers like Capella and Umbra to offer VHR SAR imagery at resolutions higher than 1 meter per pixel. Benefiting from that progress, BRIGHT incorporates both pre-event optical imagery and post-event SAR imagery with spatial resolutions ranging from 0.3 meters to 1 meter per pixel. Such high resolution allows for detailed assessments at the individual building level, as required by emergency responders to guide targeted and effective rescue operations. Different event types are considered in BRIGHT: earthquakes, storms (hurricane, cyclone), wildfires, floods, and volcanic eruptions. These natural disasters account for 84% of the fatalities and 94% of the economic losses from 1998 to 2017 (UNDRR, 2018a). In addition to natural disasters, the BRIGHT dataset further considers disasters caused by human activity, such as accidental explosions or armed conflicts, which also pose significant threats to human life and infrastructure, can occur unexpectedly and require a rapid response (UNDRR, 2018b). The inclusion of these events ensures the dataset is comprehensive and can be used to develop robust AI models that are effective across a range of disaster scenarios. The events in BRIGHT cover 12 different regions distributed around the globe, with a focus on developing countries where external assistance is most urgently needed after a disaster. BRIGHT’s labels are multi-level annotations that distinguish between damaged and entirely destroyed buildings.

Table 1. Comparison of BRIGHT with the existing building damage assessment datasets with scale, where OA indicates whether the dataset is open access or not, and GSD is an acronym for ground sampling distance. Note that since some datasets integrate other datasets, we summarize only the largest one to avoid duplication here. For example, the BDD dataset (Adriano et al., 2021) includes the Tohoku-Earthquake-2011 dataset (Bai et al., 2018) and Palu-Tsunami-2018 dataset (Adriano et al., 2019). *Although some events in the BDD dataset (Adriano et al., 2021) have Worldview-2 images as optical EO data with a GSD of 0.5 m/pixel, its corresponding SAR image has a highest GSD of 1 m/pixel. †N is the number of events used for testing in IEEE GRSS DFC 2025, which we temporarily hide here.

Dataset	OA	Modality	GSD (m/pixel)	No. of events	Disaster type	No. of building	Granularity
ABCD (Fujita et al., 2017)	Yes	Optical EO	0.4	1	Tsunami	N/A	Image-level
(Nguyen et al., 2017)	Yes	Images on social media	N/A	1	3 natural disasters	N/A	Image-level
(Cheng et al., 2021)	Yes	UAV image	N/A	1	Hurricane	1,802	Image-level
(Xue et al., 2024)	Yes	Street-view image	N/A	1	Hurricane	2,468	Image-level
(Sun et al., 2024)	Yes	Optical and SAR EO	<1	1	Earthquake	4,029	Pixel-level
FloodNet (Rahnemoonfar et al., 2021)	Yes	UAV image	N/A	1	Flood	6,675	Pixel-level
RescueNet (Rahnemoonfar et al., 2023)	Yes	UAV image	N/A	1	Hurricane	10,903	Pixel-level
Ida-BD (Kaur et al., 2023)	No	optical EO	0.5	1	Hurricane	18,083	Pixel-level
xBD (Gupta et al., 2019)	Yes	Optical EO	<0.8	15	6 natural disasters	>700,000	Pixel-level
BDD (Adriano et al., 2021)	No	optical and SAR EO	1*-10	9	3 natural disasters	123,453	Pixel-level
BRIGHT	Yes	optical and SAR EO	0.3-1	12 + N†	5 natural disasters human-made disasters	>350,000	Pixel-level

1.1 Comparison with existing datasets

The comparison between BRIGHT and existing datasets for building damage assessment is summarized in Table 1. Most current building damage assessment datasets are limited in scale and scope due to the scarcity of disaster events, the limited availability of corresponding open-source EO data and the annotation effort (Rahnemoonfar et al., 2021; Gupta and Shah, 2021; Kaur et al., 2023). Due to the high cost and time required for pixel-level labeling, some datasets, such as those provided by (Fujita et al., 2017; Nguyen et al., 2017; Cheng et al., 2021; Xue et al., 2024), offer image-level labeling, indicating only whether an image contains damaged buildings. Although useful, this information lacks the spatial precision needed to guide specific rescue operations. The xBD dataset (Gupta et al., 2019) is currently the largest open data collection, covering six natural disasters in 15 regions with more than 700,000 building instances. However, xBD includes only optical EO data and therefore does not support all-weather disaster response. Sun et al. (2024) have created a multimodal dataset, but it is limited to a single disaster event and contains only about 4,000 building instances. The small size makes it challenging to train DL models, and significantly limits the transferability of the trained models. The dataset most similar to our work is BDD, proposed by Adriano et al. (2021). The main differences between BDD and BRIGHT are: First, BRIGHT covers more disaster events and building instances, including both natural and human-made disasters. Second, BRIGHT has higher spatial resolution; while the highest resolution of SAR images in BDD is 1 meter, BRIGHT provides finer detail with spatial resolution from 0.3 meter to 1 meter, allowing for the detection of subtle structural damage in individual buildings. Third, and perhaps most important, the re-distribution of BDD is restricted, whereas BRIGHT is an open-source dataset publicly

available to the global community. Beyond the ones listed in Table 1, there are further datasets targeted at monitoring hazardous events related to disasters, but not concerned with building damage assessment, including landslides (Ghorbanzadeh et al., 2022; Meena et al., 2023), floods (Bonafilia et al., 2020; Zhang et al., 2023) and wildfires (Artés et al., 2019; Huot et al., 2022; He et al., 2024).

1.2 Main contribution

The contributions of this paper are twofold: 1) We present BRIGHT, the first multimodal building damage dataset with a spatial resolution greater than 1 meter, and make it publicly available to the community. BRIGHT employs a combination of pre-event optical imagery and post-event SAR imagery with abundant disaster events and rich geographic diversity, thereby supporting the study of AI-based multimodal building damage mapping, especially in developing countries; 2) We evaluate a series of contemporary DL baselines on BRIGHT. The results of these experiments, along with the source code and model weights, are also made publicly available in support of future research and a benchmark for the current potential of EO-based disaster response. The trained models may serve as a basis for methodological advances or to build damage assessment pipelines for real-world applications.

2 Study areas and disaster events

We selected 12 disaster events across the globe for our BRIGHT dataset, as illustrated in Figure 2. Since both Capella and Umbra satellites were launched in 2020 and beyond, we focused on study areas where disasters occurred from 2020 onward. The selected regions are primarily in developing countries, where public administration and dis-

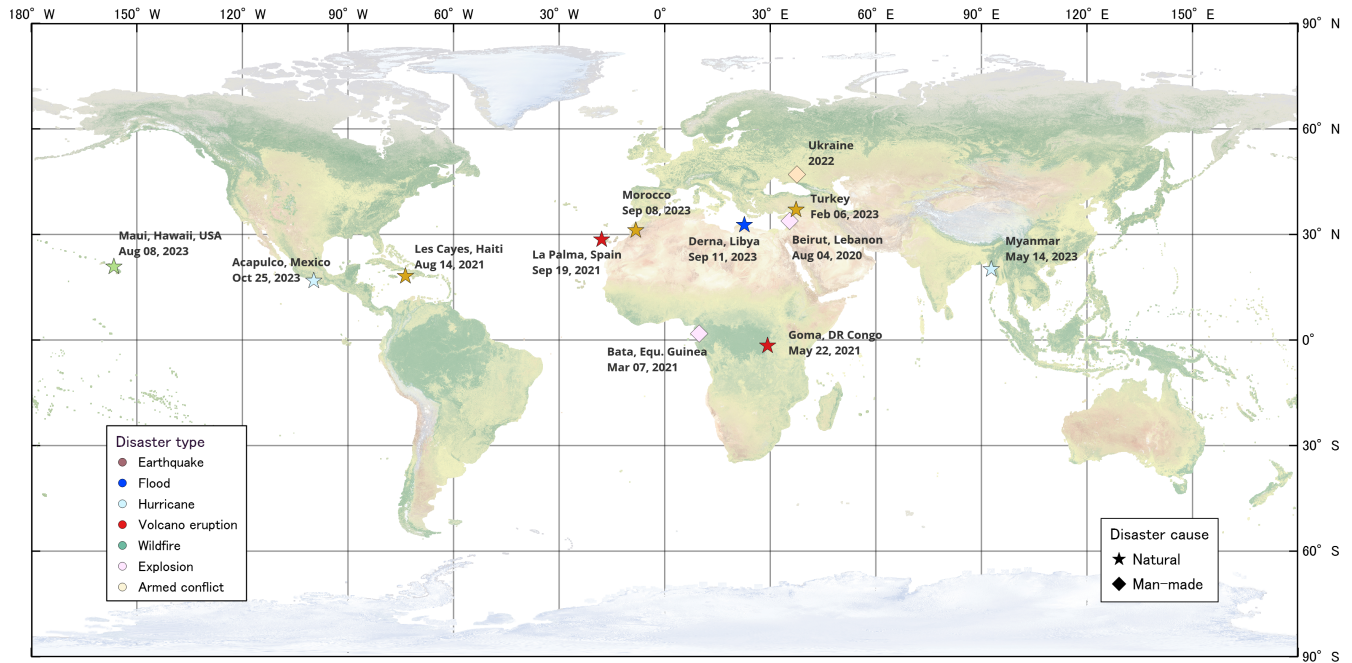


Figure 2. Geographic distribution of disaster events present in the BRIGHT. Note that **the locations of test events in IEEE GRSS DFC 2025 are hidden in this figure.**

aster response capacity tend to be weaker compared to developed nations, making international assistance more critical. The dataset covers five major types of natural disasters—earthquakes, storms (including hurricane and cyclone), wildfires, floods, and volcanic eruptions. Additionally, it includes man-made disasters such as explosions and armed conflicts.

2.1 Explosion in Beirut, 2020

On August 4, 2020, a massive explosion occurred at the Port of Beirut in Lebanon, caused by the improper storage of 2,750 tons of ammonium nitrate. The explosion caused widespread damage within a radius of several kilometers, significantly impacting the port and the surrounding neighborhoods, including areas such as Gemmayzeh, Mar Mikhael, and Achrafieh. It resulted in 218 deaths, more than 7,000 injuries, and left approximately 300,000 people homeless. Economic losses were estimated to be between 10 billion and 15 billion USD. The disaster compounded Lebanon’s ongoing economic challenges and contributed to political instability and social unrest.

2.2 Explosion in Bata, 2021

On March 7, 2021, a series of four explosions occurred at the Cuartel Militar de Nkoantoma in Bata, Equatorial Guinea, caused by improperly stored explosives. The blasts led to at least 107 deaths, over 615 injuries, and widespread de-

struction throughout the city. A total of 243 structures were destroyed or severely damaged, displacing many residents. Around 150 families sought refuge in temporary shelters, while others stayed with relatives. Local hospitals treated more than 500 injured individuals, and the economic impact was severe, underscoring the dangers associated with improper storage of hazardous materials.

2.3 Volcano Eruption in DR Congo and Rwanda, 2021

On May 22, 2021, Mount Nyiragongo in the Democratic Republic of the Congo erupted, causing widespread devastation. The eruption resulted in 32 deaths, the destruction of 1,000 homes, and the displacement of thousands as lava flows threatened the city of Goma. Nearly 400,000 people were evacuated due to the risk of further volcanic activity, including potential magma flow beneath Goma and nearby Lake Kivu. Despite continued seismic activity, life in Goma largely returned to normal by August 2021, although plans to relocate parts of the city remain under consideration due to the ongoing threat from the volcano.

2.4 Earthquake in Haiti, 2021

On August 14, 2021, a magnitude 7.2 earthquake struck Haiti’s Tiburon Peninsula, primarily affecting the Nippes, Sud, and Grand’Anse departments. The disaster caused over 2,200 deaths, more than 12,200 injuries, and left thousands homeless. The economic losses were significant, estimated

Table 2. Summary of the basic information of the BRIGHT dataset, with disaster events listed in chronological order. **Information on the test events for IEEE GRSS DFC 2025 is excluded from this table.**

Disaster area	Type of disaster	Date	GSD (m/pixel)	Provider	No. of tiles	No. of building
Beirut, Lebanon	Explosion (EP)	04 Aug. 2020	1	Maxar & Capella	133	25,496
Bata, Equatorial Guinea	Explosion (EP)	07 Mar. 2021	0.5	Maxar & Capella	107	8,893
Goma, DR Congo	Volcano eruption (VE)	22 May 2021	0.33	Maxar & Capella	123	18,741
Les Cayes, Haiti	Earthquake (EQ)	14 Aug. 2021	0.48	Maxar & Capella	73	18,918
La Palma, Spain	Volcano Eruption (VE)	19 Sept. 2021 - 13 Dec. 2021	0.3-0.35	IGN (Spain) & Capella	933	30,239
Ukraine	Armed conflict (AC)	22 Mar. 2022 - 21 Sept. 2022	0.6	Google Earth & Capella	848	56,770
Turkey	Earthquake (EQ)	06 Feb. 2023	0.30-0.35	Maxar & Capella & Umbra	1,114	135,033
Myanmar	Cyclone (CC)	14 May 2023	0.6	Google Earth & Capella	126	8,052
Maui, Hawaii, USA	Wildfire (WF)	08 Aug. 2023 - 09 Aug. 2023	0.6	NOAA & Capella	65	3,995
Morocco	Earthquake (EQ)	08 Sept. 2023	0.35-0.4	Maxar & Capella	567	6,269
Derna, Libya	Flood (FL)	10 Sept. 2023	0.35	Maxar & Capella	124	1,0979
Acapulco, Mexico	Hurricane (HC)	25 Oct. 2023	0.35-0.8	Google Earth & Capella	325	18,437
Test events of IEEE DFC 2025	N/A	N/A	N/A	N/A	N/A	N/A
<i>Total</i>	-	-	-	-	>4,538	>350,000

at over USD 1.5 billion. Approximately 137,500 buildings including homes, schools, and hospitals, were damaged or destroyed. As the deadliest natural disaster of 2021, the earthquake exacerbated Haiti's existing challenges, including widespread poverty and political instability.

2.5 Volcano Eruption in La Palma, 2021

On September 19, 2021, the Cumbre Vieja volcano on La Palma, part of Spain's Canary Islands, erupted following several days of seismic activity. The eruption primarily impacted the island's western side, covering over 1,000 hectares with lava and destroying more than 3,000 buildings, including the towns of Todoque and La Laguna. The lava flow, measuring about 3.5 kilometers wide and 6.2 kilometers long, reached the sea, cutting off the coastal highway and forming a new peninsula with extensive lava tubes. Although the timely evacuation of around 7,000 people prevented major casualties, one person died from inhaling toxic gases. Economic losses exceeded 800 million euros, and thousands of residents were displaced, with significant damage to arable land and livelihoods.

2.6 Armed Conflict in Ukraine, 2022

In February 2022, the conflict in Ukraine escalated significantly when Russian forces launched a full-scale invasion. The invasion has affected many parts of Ukraine, especially the eastern regions and the major cities, causing widespread destruction to homes, infrastructure, and industrial facilities. The conflict has resulted in thousands of civilian and military casualties and has caused the displacement of millions of people. Out of a population of 41 million, about 8 mil-

lion Ukrainians were internally displaced, while more than 8.2 million fled the country by April 2023, creating Europe's largest refugee crisis since World War II. The economic losses are substantial, with extensive damage to infrastructure, industrial output, and the broader economy.

2.7 Earthquake in Turkey, 2023

On February 6, 2023, a magnitude 7.8 earthquake struck southeastern Turkey near Gaziantep, followed by a magnitude 7.7 aftershock. The disaster, the most powerful earthquake in Turkey since 1939, caused widespread destruction across approximately 350,000 km^2 , affecting 14 million people and displacing 1.5 million. The death toll reached 53,537 in Turkey and 5,951 in Syria, with 107,213 injuries, making it one of the deadliest earthquakes in modern history. Economic losses were estimated at USD 148.8 billion in Turkey and USD 14.8 billion in Syria, with over 518,000 houses and 345,000 apartments destroyed. The earthquake caused severe damage to infrastructure, agriculture, and essential services, further worsening the region's economic challenges. International aid was mobilized to support the affected populations.

2.8 Cyclone in Myanmar, 2023

In May 2023, Cyclone Mocha, a Category 4 hurricane, struck Myanmar, causing widespread devastation in the country's coastal regions, particularly in Rakhine State. The storm resulted in at least 460 deaths, with over 700 people injured, mostly among the Rohingya refugees. The cyclone destroyed over 183,000 houses, 1,770 religious buildings, and 1,397 schools, and caused US\$2.24 billion in damages, equivalent to 3.4% of Myanmar's GDP. Severe flooding affected 895

km^2 of land, displacing over 1.2 million people. In Rakhine, towns like Sittwe were heavily flooded, with a storm surge of up to 3.5 meters, while nearly 90% of homes in Kyauktaw were destroyed. The cyclone severely affected communication networks and infrastructure, exacerbating the region's vulnerability to future natural disasters.

2.9 Wildfire in Hawaii, 2023

In August 2023, a series of wildfires broke out on the island of Maui, Hawaii, causing widespread destruction and significant impacts on the local population and environment. The fires, fueled by dry conditions and strong winds, primarily affected the town of Lahaina, where at least 102 people were killed and two remain missing. Over 2,200 buildings were destroyed, including many historic landmarks, resulting in estimated damages of US\$5.5 billion. The fires prompted evacuations and led to the displacement of thousands of residents, with significant economic losses in the tourism and agriculture sectors.

2.10 Earthquake in Morocco, 2023

On September 8, 2023, a 6.9 magnitude earthquake struck Morocco's Al Haouz Province, near Marrakesh, causing widespread devastation. The quake resulted in at least 2,960 deaths and 5,674 injuries, affecting over 2.8 million people, including 100,000 children. The earthquake damaged or destroyed 40,759 houses and 2,930 villages, with 19,095 additional houses collapsing. Significant destruction occurred in rural areas of the Atlas Mountains. Economic losses could reach up to 9% of Morocco's GDP. Historic sites in Marrakesh, including parts of the Medina and several mosques, were severely damaged.

2.11 Flood and Storm in Libya, 2023

In September 2023, northeastern Libya was hit by Storm Daniel, causing catastrophic flooding, particularly in the city of Derna. The storm led to the collapse of two dams, releasing 30 million cubic meters of water and partially destroying the city. Casualty estimates range from 5,900 to 20,000, making it the second deadliest dam failure in history. The flooding affected seven out of 10 districts in Derna and left more than 40,000 people displaced. More than 2,200 buildings were flooded and the collapse of four bridges split the city into two. The economic losses were substantial, with severe damage to infrastructure, homes, and the agricultural sector.

2.12 Hurricane in Mexico, 2023

In September 2023, Hurricane Norma, a Category 4 hurricane, struck the western coast of Mexico, severely affecting Sinaloa and Baja California Sur. The storm caused over 100 deaths and displaced thousands, with significant damage to

homes, infrastructure, and agriculture. This was followed by Hurricane Otis in October, which made landfall near Acapulco as a Category 5 hurricane. Otis was the strongest Pacific hurricane to hit Mexico, causing at least 52 deaths and leaving 32 missing. The storm caused unprecedented destruction, with more than 51,864 homes destroyed and damages estimated at US\$12–16 billion, surpassing Hurricane Wilma as the costliest Mexican hurricane.

3 Dataset Description

3.1 Construction of the dataset

The optical EO data in our dataset are mainly from Maxar's Open Data program¹, while the SAR EO data are mainly from Capella Space and Umbra Space. Both Capella and Umbra data have two imaging modalities, *i.e.*, Spotlight and Stripmap, respectively. The Spotlight mode has a higher spatial resolution but less coverage. In the region of interest, we preferred Spotlight mode if there is suitable data in the data provider's inventory, otherwise, we chose Stripmap. The optical EO data consist of red, blue, and green bands, while the SAR EO data are mainly amplitude data in the VV or HH bands. For optical EO data, the digital number was converted to reflectance and then standardized to an 8-bit data format. For SAR imagery, after the data have been terrain-corrected, we used the data provider's recommended method of pre-processing the amplitude data and finally converted the same to an 8-bit data format. Although both optical and SAR images are geocoded, there is still some pixel offset between them. Therefore, multiple experts manually aligned the paired optical and SAR data and cross-checked each other to ensure the precise registration between the two types of EO data.

The labels in BRIGHT consist of two components: building polygons and post-disaster building damage attributes. Expert annotators manually labeled the building polygons, and all labels underwent independent visual inspections to ensure accuracy. Damage annotations were obtained from Copernicus Emergency Management Service² and the United Nations Satellite Centre (UNOSAT)³ Emergency Mapping Products. These annotations were derived through visual interpretation of high-resolution optical imagery captured before and after the disasters by EO experts, supplemented by partial field visits. Since the number of damage levels varied across different events, we adopted the approach in (Adriano et al., 2021) to standardize them into three categories: intact, damaged, and destroyed. The damage annotations were provided as vector point files. By overlaying these points with the building polygons and assigning corresponding damage attributes, we generated the final building

¹<https://www.maxar.com/open-data>

²<https://emergency.copernicus.eu>

³<https://unosat.org/products>

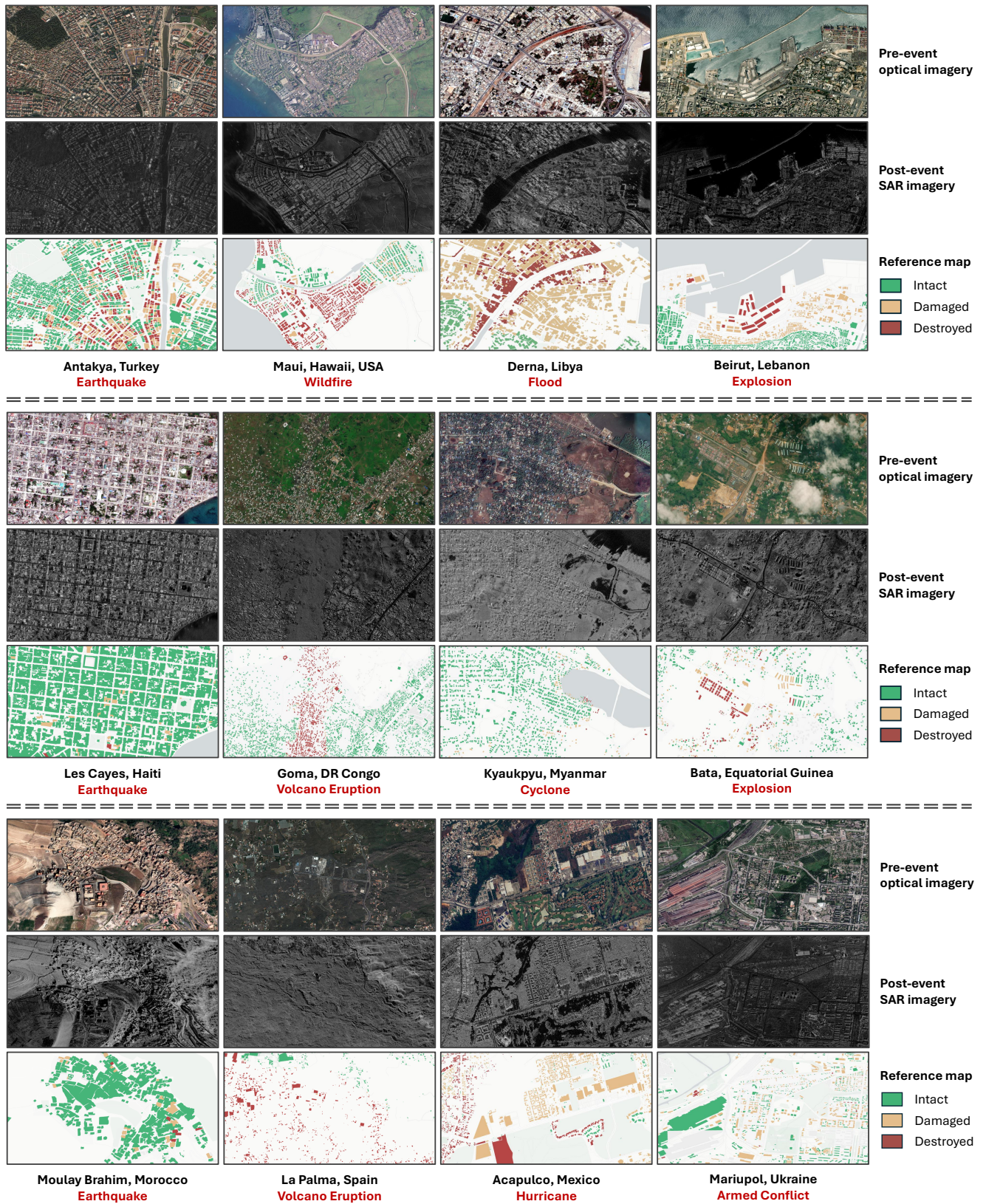


Figure 3. Thumbnails of local areas in 12 disaster events of BRIGHT. For visualization purposes, different events have different scales.

damage labels. To prevent geographic misallocations due to coordinate offsets, we unified the coordinate systems of the points and polygons, with a visual inspection performed prior to the final allocation.

Figure 3 presents thumbnails of selected local areas from the 12 disaster events included in the BRIGHT dataset.

3.2 Statistics for BRIGHT

The basic information about BRIGHT, including disaster events, EO data, the number of corresponding EO tiles, and the total number of building pixels, is summarized in Table 2. After cropping the EO data into 1024×1024 -pixel tiles, BRIGHT contains 4,538 multimodal image pairs (excluding events related to IEEE GRSS DFC 2025). As BRIGHT covers different disaster events located in different regions across the globe, this ensures the geographical diversity of its sample.

Key statistics of BRIGHT are illustrated in Figure 4. Figure 4a shows the pixel value distribution for optical and SAR images from one man-made disaster and three natural disasters. The varying geographical landscapes and land cover across different regions result in distinct means and standard deviations of pixel values, highlighting BRIGHT’s geographical diversity and making it a robust dataset for studying building damage assessment in diverse environments. To ensure trained deep learning (DL) models can accurately detect buildings and assess damage levels, it is crucial that the dataset includes a wide variety of building styles from different regions. Figure 4b shows that BRIGHT covers buildings at multiple scales, exhibiting a “long-tail” distribution. This multi-scale representation challenges DL models to develop the ability to capture features at varying scales, enhancing robustness and accuracy.

Figure 4c further illustrates the feature distribution of buildings in optical and SAR images for the same four events shown in Figure 4a, demonstrating clear inter-event separability in both modalities. Finally, BRIGHT faces a significant challenge of sample imbalance. There is a notable imbalance between background pixels and foreground (building) pixels, with a ratio of approximately 7:1. Additionally, an imbalance exists within damage categories: only about 6.5% of building pixels represent destroyed buildings, 6.7% correspond to damaged buildings, and 86.8% are intact buildings. This imbalance complicates model training, necessitating careful strategies to develop robust DL models.

We also evaluated the alignment errors between optical and SAR EO data in BRIGHT. Table 3 presents the mean co-registration errors, measured in root mean square error (RMSE) of pixel displacement, obtained using three different multimodal image registration methods: RIFT (Li et al., 2020), SRIF (Li et al., 2023a), and LNIFT (Li et al., 2022). The evaluation resulted in an RMSE of about 1.5 pixels between optical and SAR EO data. This enhanced alignment

Table 3. Mean co-registration errors obtained from different multimodal image registration methods.

Descriptor	RMSE (pixels)
RIFT (Li et al., 2020)	1.935
LNIFT (Li et al., 2022)	0.905
SRIF (Li et al., 2023a)	1.790
Average	1.543

provides a fundamental guarantee for accurate building damage assessment in BRIGHT.

3.3 Dataset division strategy

To train ML/DL models using BRIGHT and evaluate their generalizability, it is necessary to divide the dataset into a training set, validation set, and test set. Gerard et al. (2024) suggested that dividing the dataset on an event-by-event basis, rather than randomly across the entire dataset, provides a more accurate reflection of a model’s generalizability. Therefore, for the first 12 events listed in Table 2, we divide the corresponding data for each event into training, validation, and test sets in a ratio of 7:1:2. The sets obtained for each event are then merged to create the final training, validation, and test sets. In our experiments, DL models are trained using the training set, and the optimal hyperparameters (e.g., learning rate) are selected based on performance on the validation set. The generalization capability of the models is subsequently evaluated on the test set.

4 Methodology

4.1 Problem statement and two solutions

The objective of building damage assessment is to interpret EO data covering the affected area and generate a building damage proxy map that reflects the extent of damage to buildings. To achieve this, two common solutions are typically employed.

One is to directly treat the building damage assessment task as a single semantic segmentation task (Adriano et al., 2021; Gupta and Shah, 2021). The pre- and post-event images are taken as inputs of the model, and then the final damage proxy map is directly predicted, which can be formalized as $\mathbf{Y}^{dam} = \mathcal{M}^{seg}(\mathbf{X}^{T_1}, \mathbf{X}^{T_2})$, where \mathbf{X}^{T_1} is the pre-event imagery, \mathbf{X}^{T_2} is the post-event imagery, $\mathcal{M}^{seg}(\cdot)$ is a semantic segmentation model, \mathbf{Y}^{dam} is the obtained damage proxy map. In the context of this paper, \mathbf{X}^{T_1} is VHR optical imagery and \mathbf{X}^{T_2} is VHR SAR imagery.

The second solution adopts the task decoupling approach (Gupta et al., 2019; Zheng et al., 2021), which breaks down building damage assessment into two subtasks: the building localization task, *i.e.*, separating the building from the

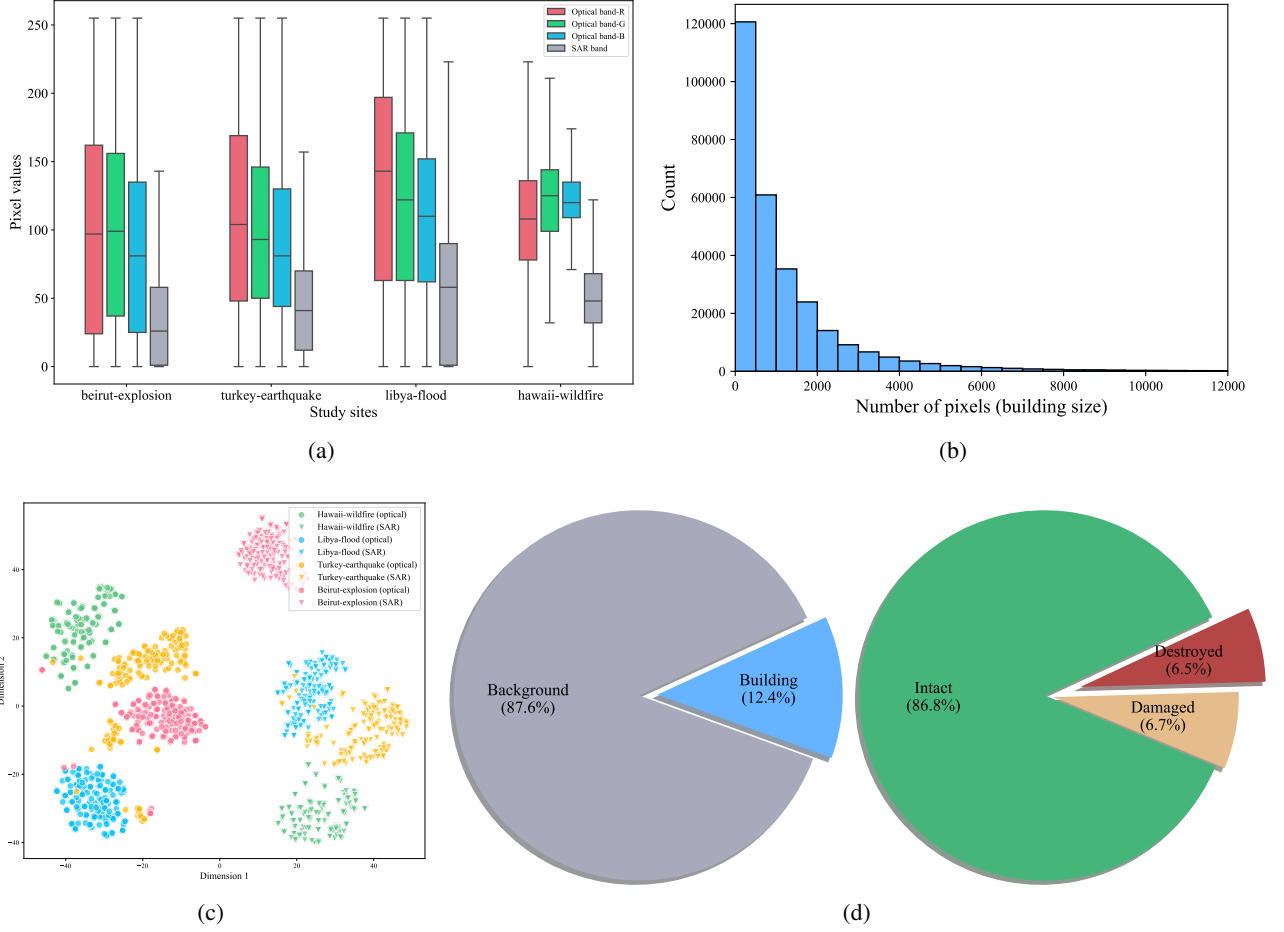


Figure 4. Statistics for the BRIGHT dataset. (a) Distributions of band values of samples from four study sites. (b) Distribution of building scales. (c) Feature distribution of buildings on four events under two imaging modalities. (d) Percentage of building and background pixels (left) and percentage of different damage levels in building pixels (right).

background, and the damage classification task, *i.e.*, focusing on the classification between different levels of damage. This solution can be formulated as $\mathbf{Y}^{loc} = \mathcal{M}^{loc}(\mathbf{X}^{T_1})$ and $\mathbf{Y}^{clf} = \mathcal{M}^{clf}(\mathbf{X}^{T_1}, \mathbf{X}^{T_2})$, where \mathbf{Y}^{loc} is the building localization map, \mathbf{Y}^{clf} is the damage classification map, $\mathcal{M}^{loc}(\cdot)$ and $\mathcal{M}^{clf}(\cdot)$ are models for building localization and damage classification tasks, respectively. $\mathcal{M}^{loc}(\cdot)$ and $\mathcal{M}^{clf}(\cdot)$ can be two separate models (Gupta et al., 2019) or a unified multi-task learning model (Zheng et al., 2021; Chen et al., 2022, 2024). The final building damage proxy map is obtained by combining the two outputs using a simple mask operation: $\mathbf{Y}^{dam} = \mathbf{Y}^{loc} \odot \mathbf{Y}^{clf}$.

Since the aim of this article is not only to provide a large-scale multimodal benchmark dataset to support all-weather disaster response but also to offer insights for designing appropriate methods in future research, we will employ and compare both solutions in our experiments.

4.2 Deep learning architecture

We evaluate BRIGHT using several advanced deep network architectures from both the computer vision and remote sensing communities. Since the building damage assessment task can be considered a specialized semantic segmentation task, we selected two well-known segmentation networks from the computer vision field: UNet (Ronneberger et al., 2015) and DeepLabV3+ (Chen et al., 2018). Additionally, we included several state-of-the-art networks from the EO community: SiamAttnUNet (Adriano et al., 2021), SiamCRNN (Chen et al., 2020), ChangeOS (Zheng et al., 2021), DamageFormer (Chen et al., 2022), and ChangeMamba (Chen et al., 2024). These networks encompass a broad range of deep learning paradigms, including CNNs, RNNs, Transformers, and the more recent Mamba architecture.

Among these seven networks, UNet, DeepLabV3+, and SiamAttnUNet adopt the first solution, directly treating building damage assessment as a single semantic segmen-

tation task. In contrast, SiamCRNN, ChangeOS, DamageFormer, and ChangeMamba adopt the second solution by decoupling the task into two subtasks: building localization and damage classification.

4.3 Model training

To train these models, we use a combination of cross-entropy loss and Lovasz softmax loss (Berman et al., 2018). Cross-entropy loss serves as the basic loss function for dense prediction tasks, while Lovasz softmax loss effectively addresses sample imbalance, between non-building and building pixels, and across different damage levels.

For UNet, DeepLabV3+, and SiamAttnUNet, which directly predict damage proxy maps from the input multimodal image pairs, the training loss function is defined as:

$$\mathcal{L}_{coupled}^{bda} = \mathcal{L}_{ce}^{bda} + \mathcal{L}_{lov}^{bda}. \quad (1)$$

For SiamCRNN, ChangeOS, DamageFormer, and ChangeMamba, which decouple building damage assessment into building localization and damage classification subtasks, the training loss function is defined as:

$$\mathcal{L}_{decoupled}^{bda} = \mathcal{L}_{ce}^{loc} + \mathcal{L}_{lov}^{loc} + \mathcal{L}_{ce}^{clf} + \mathcal{L}_{lov}^{clf}. \quad (2)$$

All models are trained using the AdamW optimizer (Loshchilov and Hutter, 2017) with a learning rate of $1e^{-4}$ and a weight decay of $5e^{-3}$. The training process consists of 50,000 iterations, with a batch size of 16. To enhance sample diversity and improve model generalization, we apply several data augmentation techniques, including random flipping, random rotation (in 90-degree increments), and random cropping.

4.4 Accuracy assessment

We adopt overall accuracy (OA), F1 score (F1), and mean intersection over union (mIoU) to evaluate the performance of DL models on building damage assessment. These metrics are commonly used in previous research on building damage assessment (Zheng et al., 2021). Following the setup in prior unimodal building damage assessment studies and the related xView2 Challenge (Gupta et al., 2019), F1 score is used to assess the performance of DL models in the building localization and damage classification subtasks. Finally, OA and mIoU are employed to measure the overall quality of the final damage proxy map, providing a comprehensive assessment of the models' ability to localize buildings and classify damage levels accurately.

5 Results and Discussions

5.1 BRIGHT evaluation results

Table 4 shows the evaluation results for each model on the test set. We observe that ChangeMamba achieves the best

overall performance, with an OA of 96.65%, an mIoU of 67.19%, and the highest F_1^{loc} and F_1^{clf} scores (91.60% and 67.93%, respectively). DamageFormer also performs well, closely following ChangeMamba, with an mIoU of 66.86% and an OA of 96.49%. Both models demonstrate strong capability in both building localization and damage classification tasks. The accuracy advantage of ChangeMamba and DamageFormer underscores the importance of leveraging advanced deep learning architectures to improve performance in complex tasks such as building damage assessment. For models using the direct prediction approach (UNet, DeepLabV3+, SiamAttnUNet), DeepLabV3+ delivers the best results, with an mIoU of 62.92% and an OA of 95.59%. However, its performance still lags behind that of the decoupled models, further emphasizing the advantage of task decoupling.

In order to ensure that the evaluation is not dominated by a few events with a large number of images (like Turkey-Earthquake-2023), Table 5 further presents the event-level mIoU for each model across 9 of 12 disaster events. ChangeMamba and DamageFormer achieve the highest average mIoU, with scores of 55.45% and 56.18%, respectively. Notably, DamageFormer performs particularly well on events such as Goma-VE-2022, La Palma-VE-2021, and Derna-FL-2023, demonstrating its robustness across different types of disasters. While performance varies across events, earthquake-related events such as Les Cayes-EQ-2021, Morocco-EQ-2023, and Turkey-EQ-2023 present greater challenges for all models, where the average mIoU remains relatively low. This highlights the need for further research to improve model robustness for earthquake damage assessment, where damage patterns are often more complex and diverse.

Finally, Figure 5 shows some of the building damage proxy maps obtained by the seven models on the test set.

5.2 Limitation of BRIGHT

The performance of ML/DL models heavily depends on the quality of the training data. The BRIGHT dataset is designed to enable ML/DL models trained on it to generate building damage proxy maps of practical significance for future disaster events. It is anticipated that BRIGHT will serve as a benchmark for numerous subsequent studies and practical disaster relief applications.

However, the BRIGHT dataset also has some limitations. Firstly, our dataset involves both optical and SAR imagery covering the same locations. SAR images, in particular, can be distorted and stretched in certain areas. Despite thorough preprocessing, including manual alignment and cross-checking by multiple experts in EO data processing, minor alignment errors may still persist, as suggested by Table 3. Secondly, the building polygons in BRIGHT were manually annotated by expert annotators. Although manual labeling generally ensures high accuracy, minor errors in polygon

Table 4. Accuracy assessment for different DL models on the set-level. The highest values are highlighted in **red**, and the second-highest results are highlighted in **blue**.

Method	F_1^{loc} (%)	F_1^{clf} (%)	Final OA (%)	Final mIoU (%)	IoU per class (%)			
					Background	Intact	Damaged	Destroyed
UNet	89.19	54.69	94.73	59.74	96.16	69.84	17.64	55.32
DeepLabV3+	87.69	59.77	95.59	62.92	95.80	74.21	22.63	59.03
SiamAttnUNet	88.90	58.93	95.47	62.76	96.13	73.94	19.91	61.08
SiamCRNN	90.39	63.56	96.20	65.23	96.55	77.42	26.26	60.68
ChangeOS	90.55	65.99	96.20	65.69	96.54	77.58	28.36	60.27
DamageFormer	90.98	66.44	96.49	66.86	96.84	79.08	28.64	62.90
ChangeMamba	91.60	67.93	96.65	67.19	97.07	80.16	30.35	61.19

Table 5. The mIoU on different events for different DL models. The highest values are highlighted in **purple**, and the second-highest results are highlighted in **teal**.

Events	UNet	DeepLabV3+	SiamAttnUNet	SiamCRNN	ChangeOS	DamageFormer	ChangeMamba
Beirut-EP-2020	52.43	39.84	46.48	49.97	48.15	55.04	50.05
Bata-EP-2021	46.42	58.02	41.99	58.34	58.00	60.80	59.84
Goma-VE-2022	58.80	60.10	62.06	60.34	61.34	62.75	58.90
Les Cayes-EQ-2021	40.07	39.37	40.03	41.34	41.40	41.76	42.18
La Palma-VE-2021	61.59	62.89	66.47	65.58	62.75	65.67	65.36
Ukraine-AC-2022	-	-	-	-	-	-	-
Turkey-EQ-2023	48.91	48.87	50.93	50.93	53.12	52.60	54.14
Myanmar-CC-2023	-	-	-	-	-	-	-
Hawaii-WF-2023	46.68	54.29	47.71	58.36	60.40	60.25	59.43
Morocco-EQ-2023	42.41	40.54	42.62	42.98	43.15	43.91	44.43
Derna-FL-2023	50.05	53.17	60.50	59.40	58.45	62.86	64.68
Acapulco-HC-2023	-	-	-	-	-	-	-
Average	49.71	50.79	50.98	54.14	54.08	56.18	55.45

boundaries are inevitable due to the complexity of building shapes and the variability in image resolution. These inaccuracies may slightly affect the performance of the models trained on BRIGHT. Then, the extent of damage to buildings is assessed by experts through visual interpretation of optical EO data. This process is susceptible to occasional misjudgments, contributing to label noise. Finally, although BRIGHT is globally distributed and richly geographically diverse, it has the problem of regional imbalance in the number of labels. Some of its events have more tiles and building numbers and thus are more dominant in training and evaluation, e.g., Turkey-Earthquake-2023 *v.s.* Hawaii-Wildfire-2023 in Table 2.

Overall, despite the limitations, it is the first time such a multimodal VHR dataset has been constructed that caters to a transferable approach to obtain building damage proxy maps at different geographical locations.

5.3 Significance of BRIGHT

Latency in responding to disaster events often arises from delays in interpretation methods and the acquisition of EO data (Ye et al., 2024). Traditionally, building damage proxy maps are generated through expert visual interpretation, a time-consuming process. Although ML- and DL-based methods offer automated and efficient approaches to building damage proxy mapping, they are often limited by the available training data. Large open-source optical datasets, though valuable, restrict models to optical imagery alone. The acquisition of clean optical EO data also requires sunlight and a cloud-free environment, which can result in delays of several days for certain disaster events such as typhoons and wildfires. As the first globally distributed multimodal dataset, BRIGHT encompasses both pre-event optical imagery and post-event SAR imagery. This unique combination overcomes the limitations of optical EO data by enabling models trained on BRIGHT to monitor disaster-stricken areas

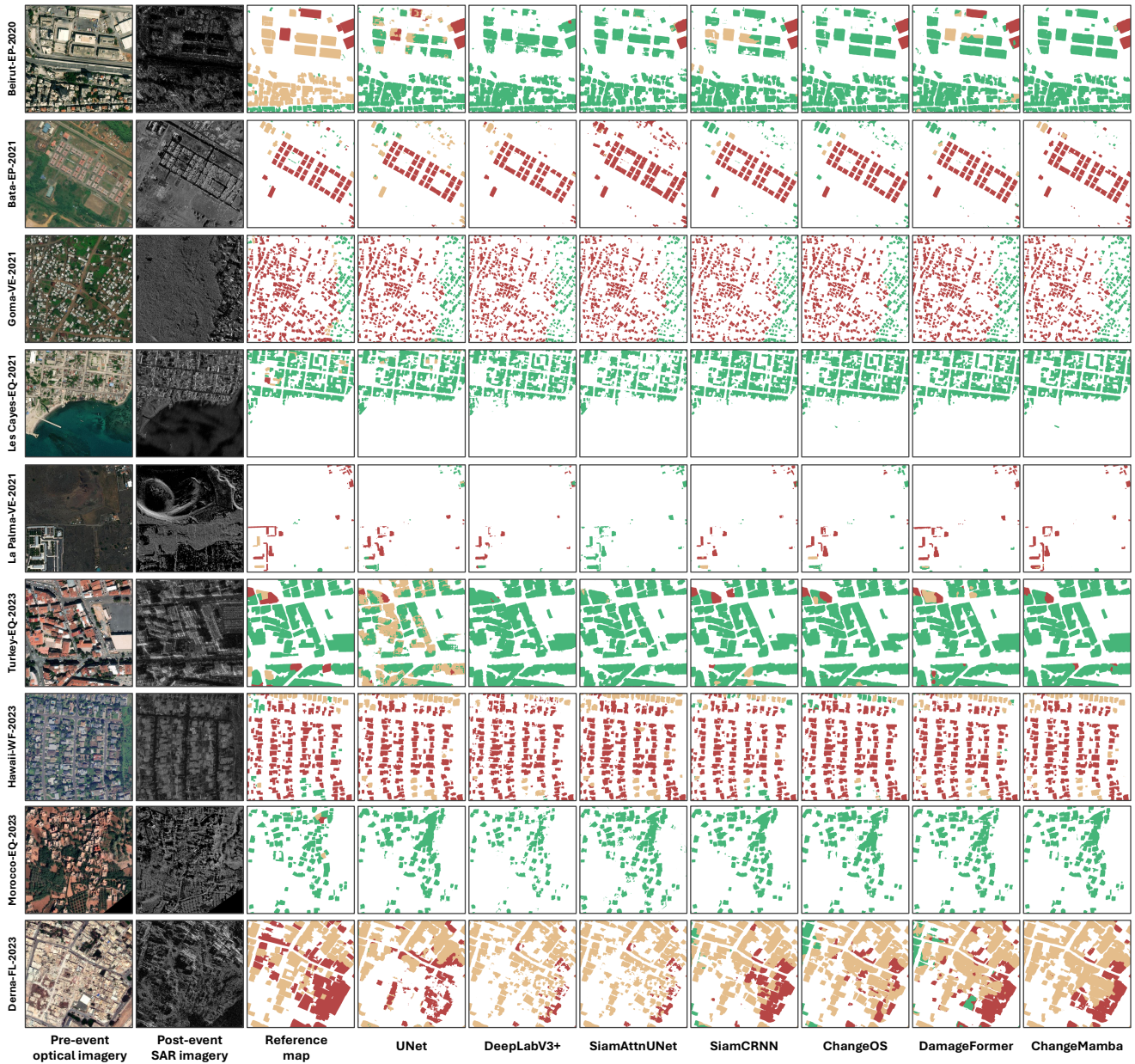


Figure 5. Damage proxy maps for different models on the test images of 9 events. The meaning of the color in reference maps and damage proxy maps is consistent with Figure 3.

regardless of weather conditions or daylight. Compared to existing building damage datasets, BRIGHT offers several distinct characteristics: multimodal data, VHR imagery with resolutions better than 1 meter per pixel, coverage of six types of natural disasters, as well as man-made disasters, rich geographic diversity, and open access to the community. Due to these features, BRIGHT is anticipated to serve as a benchmark for many subsequent studies and practical disaster relief applications. BRIGHT facilitates research on building damage assessment. Looking forward, BRIGHT can be expanded to include additional data modalities such as height

data, which would provide valuable topographic information to enhance disaster response strategies. Incorporating more bands in optical and SAR data could also broaden the applicability of the dataset.

In addition to its primary application in building damage assessment, the BRIGHT dataset holds significant potential for other domains, particularly in multimodal EO data-related research. Firstly, BRIGHT can be directly used for as a building detection benchmark dataset with a rich geographic diversity and building patterns. Beyond that, researchers can also leverage BRIGHT to generate new

datasets tailored to specific needs to explore new techniques including, but not limited to, image registration, land cover change detection, land cover mapping, height estimation, EO-driven visual question answering (VQA), improving the performance and reliability of models in complex environments. Moreover, BRIGHT can become an invaluable resource for the development of remote sensing foundation models (Wang et al., 2023; Hong et al., 2024). These emerging models, designed to generalize across various tasks and datasets, benefit immensely from the rich multimodal data and extensive geographic diversity offered by BRIGHT. By incorporating both optical and SAR data, BRIGHT enables the pre-training of more robust foundation models capable of handling the complexities of real-world remote sensing applications. This contribution is particularly important as the field moves towards creating versatile, scalable AI models that can be applied across different types of EO data and disaster scenarios (Li et al., 2024). We envision that BRIGHT, true to its name, will bring even a glimmer of bright to people in disaster-stricken areas by enabling more prompt and effective disaster response and relief.

6 Conclusions

A prompt and comprehensive understanding of building damage following a disaster is critical for effective disaster response and relief operations. Currently, large-scale optical datasets support the development of automated ML/DL methods, but their use is limited by weather conditions and daylight availability. In contrast, all-weather disaster response can be facilitated by leveraging multimodal EO data. In this paper, we introduced BRIGHT, the first globally distributed, multimodal dataset with open access to the community, covering 12 natural and man-made disaster events. BRIGHT includes pre-event optical imagery and post-event SAR imagery with very high spatial resolutions (better than 1 meter). Alongside the dataset, we evaluated several state-of-the-art models on BRIGHT. The experimental results demonstrate the effectiveness of BRIGHT in mapping building damage across unseen events. These findings provide both performance baselines and valuable insights into model design for future research. BRIGHT is an ongoing project, and we remain committed to continuously enhancing its diversity and quality by incorporating new disaster events and refining the existing data. Our objective is to further improve BRIGHT's utility for future research within the community and for practical disaster response applications at regional, national, and international levels.

7 Code and data availability

The BRIGHT dataset and the code for training and testing benchmark methods (including code related to IEEE

GRSS DFC 2025) are available at <https://github.com/ChenHongruixuan/BRIGHT>.

Author contributions. **Hongruixuan Chen:** conceptualization (lead), data curation (lead), funding acquisition (equal), methodology (lead), project administration (lead), investigation (lead), software (lead), writing – original draft preparation (lead), visualization (lead). **Jian Song:** conceptualization (support), data curation (equal), funding acquisition (support), investigation (support), writing – original draft preparation (equal), visualization (support). **Olivier Dietrich:** conceptualization (support), data curation (equal), software (support), visualization (equal), writing – review and editing (support). **Clifford Broni-Bediako:** conceptualization (support), data curation (support), writing – review and editing (equal). **Weihao Xuan:** data curation (support), project administration (support), writing – review and editing (support). **Junjue Wang:** data curation (support), writing – review and editing (support). **Xinlei Shao:** funding acquisition (support), writing – review and editing (support). **Yimin Wei:** writing – review and editing (support). **Junshi Xia:** conceptualization (support), data curation (support), supervision (support), writing – review and editing (support). **Cuiling Lan**⁴: conceptualization (support), supervision (support), writing – linguistic refinement (equal). **Konrad Schindler:** conceptualization (equal), resources (support), supervision (equal), writing – review and editing (equal). **Naoto Yokoya:** conceptualization (equal), funding acquisition (lead), resources (lead), supervision (lead), writing – review and editing (equal).

Competing interests. The contact author has declared that none of the authors has any competing interests.

Acknowledgements. This work was supported in part by the JSPS, KAKENHI under Grant Number 24KJ0652 and 22H03609, the Council for Science, Technology and Innovation (CSTI), the Cross-ministerial Strategic Innovation Promotion Program (SIP), Development of a Resilient Smart Network System against Natural Disasters (Funding agency: NIED), JST, FOREST under Grant Number JPMJFR206S, Microsoft Research Asia, Next Generation AI Research Center of The University of Tokyo, and Young Researchers Exchange Programme between Japan and Switzerland under the Japanese-Swiss Science and Technology Programme. The authors would also like to give special thanks to Sarah Preston of Capella Space, Capella Space's Open Data Gallery, Maxar Open Data Program and Umbra Space's Open Data Program for providing the valuable data.

References

Adriano, B., Xia, J., Baier, G., Yokoya, N., and Koshimura, S.: Multi-Source Data Fusion Based on Ensemble Learning for Rapid Building Damage Mapping during the 2018 Sulawesi

⁴Cuiling Lan did not participate in any activities related to the acquisition, processing, utilization, or distribution of the datasets. Her access to the data was solely limited to the information presented in the current paper, similar to that of the readers.

- Earthquake and Tsunami in Palu, Indonesia, *Remote Sensing*, 11, 2019.
- Adriano, B., Yokoya, N., Xia, J., Miura, H., Liu, W., Matsuoka, M., and Koshimura, S.: Learning from multimodal and multitemporal earth observation data for building damage mapping, *ISPRS J. Photogramm. Remote Sens.*, 175, 132–143, 2021.
- Arciniegas, G. A., Bijker, W., Kerle, N., and Tolpekin, V. A.: Coherence- and Amplitude-Based Analysis of Seismogenic Damage in Bam, Iran, Using ENVISAT ASAR Data, *IEEE Transactions on Geoscience and Remote Sensing*, 45, 1571–1581, 2007.
- Artés, T., Oom, D., de Rigo, D., Durrant, T. H., Maianti, P., Libertà, G., and San-Miguel-Ayanz, J.: A global wildfire dataset for the analysis of fire regimes and fire behaviour, *Scientific Data*, 6, 296, 2019.
- Bai, Y., Adriano, B., Mas, E., and Koshimura, S.: Machine Learning Based Building Damage Mapping from the ALOS-2/PALSAR-2 SAR Imagery: Case Study of 2016 Kumamoto Earthquake, *Journal of Disaster Research*, 12, 646–655, 2017.
- Bai, Y., Gao, C., Singh, S., Koch, M., Adriano, B., Mas, E., and Koshimura, S.: A Framework of Rapid Regional Tsunami Damage Recognition From Post-event TerraSAR-X Imagery Using Deep Neural Networks, *IEEE Geoscience and Remote Sensing Letters*, 15, 43–47, 2018.
- Berman, M., Triki, A. R., and Blaschko, M. B.: The Lovász-Softmax Loss: A Tractable Surrogate for the Optimization of the Intersection-Over-Union Measure in Neural Networks, in: *Proceedings of the IEEE Conference on Computer Vision and Pattern Recognition (CVPR)*, 2018.
- Bonafilia, D., Tellman, B., Anderson, T., and Issenberg, E.: Sen1Floods11: A Georeferenced Dataset to Train and Test Deep Learning Flood Algorithms for Sentinel-1, in: *Proceedings of the IEEE/CVF Conference on Computer Vision and Pattern Recognition (CVPR) Workshops*, 2020.
- Brett, P. T. B. and Guida, R.: Earthquake Damage Detection in Urban Areas Using Curvilinear Features, *IEEE Transactions on Geoscience and Remote Sensing*, 51, 4877–4884, 2013.
- Brunner, D., Lemoine, G., and Bruzzone, L.: Earthquake damage assessment of buildings using VHR optical and SAR imagery, *IEEE Trans. Geosci. Remote Sens.*, 48, 2403–2420, 2010.
- Chen, H., Wu, C., Du, B., Zhang, L., and Wang, L.: Change Detection in Multisource VHR Images via Deep Siamese Convolutional Multiple-Layers Recurrent Neural Network, *IEEE Trans. Geosci. Remote Sens.*, 58, 2848–2864, 2020.
- Chen, H., Nemni, E., Vallecorsa, S., Li, X., Wu, C., and Bromley, L.: Dual-Tasks Siamese Transformer Framework for Building Damage Assessment, in: *International Geoscience and Remote Sensing Symposium (IGARSS)*, pp. 1600–1603, 2022.
- Chen, H., Song, J., Han, C., Xia, J., and Yokoya, N.: ChangeMamba: Remote Sensing Change Detection With Spatiotemporal State Space Model, *IEEE Transactions on Geoscience and Remote Sensing*, 62, 1–20, 2024.
- Chen, L.-C., Zhu, Y., Papandreou, G., Schroff, F., and Adam, H.: Encoder-Decoder with Atrous Separable Convolution for Semantic Image Segmentation, in: *Computer Vision – ECCV 2018*, pp. 833–851, 2018.
- Chen, S.-W. and Sato, M.: Tsunami Damage Investigation of Built-Up Areas Using Multitemporal Spaceborne Full Polarimetric SAR Images, *IEEE Transactions on Geoscience and Remote Sensing*, 51, 1985–1997, 2013.
- Cheng, C.-S., Behzadan, A. H., and Noshadran, A.: Deep learning for post-hurricane aerial damage assessment of buildings, *Computer-Aided Civil and Infrastructure Engineering*, 36, 695–710, <https://doi.org/https://doi.org/10.1111/mice.12658>, 2021.
- Chini, M., Pierdicca, N., and Emery, W. J.: Exploiting SAR and VHR Optical Images to Quantify Damage Caused by the 2003 Bam Earthquake, *IEEE Transactions on Geoscience and Remote Sensing*, 47, 145–152, 2009.
- Chini, M., Anniballe, R., Bignami, C., Pierdicca, N., Mori, S., and Stramondo, S.: Identification of building double-bounces feature in very high resolution SAR data for earthquake damage mapping, in: *2015 IEEE International Geoscience and Remote Sensing Symposium (IGARSS)*, pp. 2723–2726, 2015.
- Fan, X., Nie, G., Deng, Y., An, J., Zhou, J., Xia, C., and Pang, X.: Estimating earthquake-damage areas using Landsat-8 OLI surface reflectance data, *International Journal of Disaster Risk Reduction*, 33, 275–283, 2019.
- Freire, S., Santos, T., Navarro, A., Soares, F., Silva, J., Afonso, N., Fonseca, A., and Tenedório, J.: Introducing mapping standards in the quality assessment of buildings extracted from very high resolution satellite imagery, *ISPRS Journal of Photogrammetry and Remote Sensing*, 90, 1–9, 2014.
- Fujita, A., Sakurada, K., Imaizumi, T., Ito, R., Hikosaka, S., and Nakamura, R.: Damage detection from aerial images via convolutional neural networks, in: *2017 Fifteenth IAPR International Conference on Machine Vision Applications (MVA)*, pp. 5–8, 2017.
- Ge, P., Gokon, H., Meguro, K., and Koshimura, S.: Study on the Intensity and Coherence Information of High-Resolution ALOS-2 SAR Images for Rapid Massive Landslide Mapping at a Pixel Level, *Remote Sensing*, 11, 2019.
- Ge, P., Gokon, H., and Meguro, K.: A review on synthetic aperture radar-based building damage assessment in disasters, *Remote Sensing of Environment*, 240, 111 693, 2020.
- Gerard, S., Borne-Pons, P., and Sullivan, J.: A simple, strong baseline for building damage detection on the xBD dataset, *arXiv preprint arXiv:2401.17271*, 2024.
- Ghorbanzadeh, O., Xu, Y., Ghamisi, P., Kopp, M., and Kreil, D.: Landslide4Sense: Reference Benchmark Data and Deep Learning Models for Landslide Detection, *IEEE Transactions on Geoscience and Remote Sensing*, 60, 1–17, 2022.
- Guo, H., Su, X., Wu, C., Du, B., and Zhang, L.: SAAN: Similarity-Aware Attention Flow Network for Change Detection With VHR Remote Sensing Images, *IEEE Transactions on Image Processing*, 33, 2599–2613, 2024.
- Gupta, R. and Shah, M.: RescueNet: Joint Building Segmentation and Damage Assessment from Satellite Imagery, in: *2020 25th International Conference on Pattern Recognition (ICPR)*, pp. 4405–4411, 2021.
- Gupta, R., Goodman, B., Patel, N., Hosfelt, R., Sajeew, S., Heim, E., Doshi, J., Lucas, K., Choset, H., and Gaston, M.: Creating xBD: A Dataset for Assessing Building Damage from Satellite Imagery, in: *Proceedings of the IEEE/CVF Conference on Computer Vision and Pattern Recognition (CVPR) Workshops*, 2019.
- He, K., Shen, X., and Anagnostou, E. N.: A global forest burn severity dataset from Landsat imagery (2003–2016), *Earth System Science Data*, 16, 3061–3081, 2024.

- Hong, D., Zhang, B., Li, X., Li, Y., Li, C., Yao, J., Yokoya, N., Li, H., Ghamisi, P., Jia, X., Plaza, A., Gamba, P., Benediktsson, J. A., and Chanussot, J.: SpectralGPT: Spectral Remote Sensing Foundation Model, *IEEE Transactions on Pattern Analysis and Machine Intelligence*, 46, 5227–5244, 2024.
- Huot, F., Hu, R. L., Goyal, N., Sankar, T., Ihme, M., and Chen, Y.-F.: Next Day Wildfire Spread: A Machine Learning Dataset to Predict Wildfire Spreading From Remote-Sensing Data, *IEEE Transactions on Geoscience and Remote Sensing*, 60, 1–13, 2022.
- Karimzadeh, S. and Mastuoka, M.: Building Damage Assessment Using Multisensor Dual-Polarized Synthetic Aperture Radar Data for the 2016 M 6.2 Amatrice Earthquake, Italy, *Remote Sensing*, 9, 2017.
- Kaur, N., Lee, C.-C., Mostafavi, A., and Mahdavi-Amiri, A.: Large-scale building damage assessment using a novel hierarchical transformer architecture on satellite images, *Computer-Aided Civil and Infrastructure Engineering*, 38, 2072–2091, 2023.
- Li, C., Hong, D., Zhang, B., Liao, T., Yokoya, N., Ghamisi, P., Chen, M., Wang, L., Benediktsson, J. A., and Chanussot, J.: Interpretable foundation models as decryptors peering into the Earth system, *The Innovation*, 5, 100682, 2024.
- Li, J., Hu, Q., and Ai, M.: RIFT: Multi-Modal Image Matching Based on Radiation-Variation Insensitive Feature Transform, *IEEE Transactions on Image Processing*, 29, 3296–3310, 2020.
- Li, J., Xu, W., Shi, P., Zhang, Y., and Hu, Q.: LNIPT: Locally Normalized Image for Rotation Invariant Multimodal Feature Matching, *IEEE Transactions on Geoscience and Remote Sensing*, 60, 1–14, 2022.
- Li, J., Hu, Q., and Zhang, Y.: Multimodal image matching: A scale-invariant algorithm and an open dataset, *ISPRS Journal of Photogrammetry and Remote Sensing*, 204, 77–88, 2023a.
- Li, T., Wang, C., Zhang, H., Wu, F., and Zheng, X.: DDFormer: A Dual-Domain Transformer for Building Damage Detection Using High-Resolution SAR Imagery, *IEEE Geoscience and Remote Sensing Letters*, 20, 1–5, 2023b.
- Liu, W. and Yamazaki, F.: Extraction of Collapsed Buildings in the 2016 Kumamoto Earthquake Using Multi-Temporal PALSAR-2 Data, *Journal of Disaster Research*, 12, 241–250, <https://doi.org/10.20965/jdr.2017.p0241>, 2017.
- Liu, W., Yamazaki, F., Gokon, H., and ichi Koshimura, S.: Extraction of Tsunami-Flooded Areas and Damaged Buildings in the 2011 Tohoku-Oki Earthquake from TerraSAR-X Intensity Images, *Earthquake Spectra*, 29, 183–200, 2013.
- Loshchilov, I. and Hutter, F.: Decoupled weight decay regularization, *arXiv preprint arXiv:1711.05101*, 2017.
- Matsuoka, M. and Yamazaki, F.: Building Damage Mapping of the 2003 Bam, Iran, Earthquake Using Envisat/ASAR Intensity Imagery, *Earthquake Spectra*, 21, 285–294, 2005.
- Matsuoka, M. and Yamazaki, F.: Comparative analysis for detecting areas with building damage from several destructive earthquakes using satellite synthetic aperture radar images, *Journal of Applied Remote Sensing*, 4, 041867, 2010.
- Matsuoka, M., Koshimura, S., and Nojima, N.: Estimation of building damage ratio due to earthquakes and tsunamis using satellite SAR imagery, in: 2010 IEEE International Geoscience and Remote Sensing Symposium, pp. 3347–3349, 2010.
- Meena, S. R., Nava, L., Bhuyan, K., Puliero, S., Soares, L. P., Dias, H. C., Floris, M., and Catani, F.: HR-GLDD: a globally distributed dataset using generalized deep learning (DL) for rapid landslide mapping on high-resolution (HR) satellite imagery, *Earth System Science Data*, 15, 3283–3298, 2023.
- Nguyen, D. T., Offi, F., Imran, M., and Mitra, P.: Damage Assessment from Social Media Imagery Data During Disasters, in: *Proceedings of the 2017 IEEE/ACM International Conference on Advances in Social Networks Analysis and Mining 2017*, p. 569–576, 2017.
- Rahnmooonfar, M., Chowdhury, T., Sarkar, A., Varshney, D., Yari, M., and Murphy, R. R.: FloodNet: A High Resolution Aerial Imagery Dataset for Post Flood Scene Understanding, *IEEE Access*, 9, 89644–89654, 2021.
- Rahnmooonfar, M., Chowdhury, T., and Murphy, R.: RescueNet: A High Resolution UAV Semantic Segmentation Dataset for Natural Disaster Damage Assessment, *Scientific Data*, 10, 913, <https://doi.org/10.1038/s41597-023-02799-4>, 2023.
- Ronneberger, O., Fischer, P., and Brox, T.: U-Net: Convolutional Networks for Biomedical Image Segmentation, in: *Medical Image Computing and Computer-Assisted Intervention – MICCAI 2015*, pp. 234–241, 2015.
- Sandhini Putri, A. F., Widyatmanti, W., and Umarhadi, D. A.: Sentinel-1 and Sentinel-2 data fusion to distinguish building damage level of the 2018 Lombok Earthquake, *Remote Sensing Applications: Society and Environment*, 26, 100724, 2022.
- Shen, Y., Zhu, S., Yang, T., Chen, C., Pan, D., Chen, J., Xiao, L., and Du, Q.: BDANet: Multiscale Convolutional Neural Network With Cross-Directional Attention for Building Damage Assessment From Satellite Images, *IEEE Transactions on Geoscience and Remote Sensing*, 60, 1–14, 2022.
- Stramondo, S., Bignami, C., Chini, M., Pierdicca, N., and Tertuliani, A.: Satellite radar and optical remote sensing for earthquake damage detection: results from different case studies, *International Journal of Remote Sensing*, 27, 4433–4447, 2006.
- Sun, Y., Wang, Y., and Eineder, M.: QuickQuakeBuildings: Post-Earthquake SAR-Optical Dataset for Quick Damaged-Building Detection, *IEEE Geoscience and Remote Sensing Letters*, 21, 1–5, 2024.
- Tong, X., Hong, Z., Liu, S., Zhang, X., Xie, H., Li, Z., Yang, S., Wang, W., and Bao, F.: Building-damage detection using pre- and post-seismic high-resolution satellite stereo imagery: A case study of the May 2008 Wenchuan earthquake, *ISPRS Journal of Photogrammetry and Remote Sensing*, 68, 13–27, 2012.
- UNDRR: Economic Losses, Poverty & Disasters: 1998–2017, Report, United Nations Office for Disaster Risk Reduction (UNDRR), <https://www.undrr.org/publication/economic-losses-poverty-disasters-1998-2017>, 2018a.
- UNDRR: Words into Action guideline: Man-made/technological hazards, Report, United Nations Office for Disaster Risk Reduction (UNDRR), <https://www.undrr.org/publication/words-action-guideline-man-made/technological-hazards>, 2018b.
- Wang, D., Zhang, Q., Xu, Y., Zhang, J., Du, B., Tao, D., and Zhang, L.: Advancing Plain Vision Transformer Toward Remote Sensing Foundation Model, *IEEE Transactions on Geoscience and Remote Sensing*, 61, 1–15, 2023.
- Wang, J., Guo, H., Su, X., Zheng, L., and Yuan, Q.: PCDAS-Net: Position-Constrained Differential Attention Siamese Network for Building Damage Assessment, *IEEE Transactions on Geoscience and Remote Sensing*, 62, 1–18, 2024.

- Wang, T.-L. and Jin, Y.-Q.: Postearthquake Building Damage Assessment Using Multi-Mutual Information From Pre-Event Optical Image and Postevent SAR Image, *IEEE Geoscience and Remote Sensing Letters*, 9, 452–456, 2012.
- Watanabe, M., Thapa, R. B., Ohsumi, T., Fujiwara, H., Yonezawa, C., Tomii, N., and Suzuki, S.: Detection of damaged urban areas using interferometric SAR coherence change with PALSAR-2, *Earth, Planets and Space*, 68, 131, 2016.
- Xia, H., Wu, J., Yao, J., Zhu, H., Gong, A., Yang, J., Hu, L., and Mo, F.: A Deep Learning Application for Building Damage Assessment Using Ultra-High-Resolution Remote Sensing Imagery in Turkey Earthquake, *International Journal of Disaster Risk Science*, 14, 947–962, 2023.
- Xie, S., Duan, J., Liu, S., Dai, Q., Liu, W., Ma, Y., Guo, R., and Ma, C.: Crowdsourcing Rapid Assessment of Collapsed Buildings Early after the Earthquake Based on Aerial Remote Sensing Image: A Case Study of Yushu Earthquake, *Remote Sensing*, 8, 2016.
- Xue, Z., Zhang, X., Prevatt, D. O., Bridge, J., Xu, S., and Zhao, X.: Post-hurricane building damage assessment using street-view imagery and structured data: A multi-modal deep learning approach, *arXiv preprint arXiv:2404.07399*, 2024.
- Yamaguchi, Y.: Disaster Monitoring by Fully Polarimetric SAR Data Acquired With ALOS-PALSAR, *Proceedings of the IEEE*, 100, 2851–2860, 2012.
- Yamazaki, F. and Matsuoka, M.: Remote Sensing Technologies in Post-Disaster Damage Assessment, *Journal of Earthquake and Tsunami*, 01, 193–210, 2007.
- Ye, S., Zhu, Z., and Suh, J. W.: Leveraging past information and machine learning to accelerate land disturbance monitoring, *Remote Sensing of Environment*, 305, 114 071, 2024.
- Yonezawa, C. and Takeuchi, S.: Decorrelation of SAR data by urban damages caused by the 1995 Hyogoken-nanbu earthquake, *International Journal of Remote Sensing*, 22, 1585–1600, 2001.
- Yusuf, Y., Matsuoka, M., and Yamazaki, F.: Damage assessment after 2001 Gujarat earthquake using Landsat-7 satellite images, *Journal of the Indian Society of Remote Sensing*, 29, 17–22, 2001.
- Zhang, J., Liu, K., and Wang, M.: Flood detection using Gravity Recovery and Climate Experiment (GRACE) terrestrial water storage and extreme precipitation data, *Earth System Science Data*, 15, 521–540, 2023.
- Zheng, Z., Zhong, Y., Wang, J., Ma, A., and Zhang, L.: Building damage assessment for rapid disaster response with a deep object-based semantic change detection framework: From natural disasters to man-made disasters, *Remote Sens. Environ.*, 265, 112 636, 2021.